Geochemistry Geophysics Geosystems G3

AN ELECTRONIC JOURNAL OF THE EARTH SCIENCES

Published by AGU and the Geochemical Society

Article

Volume 6, Number 9

10 September 2005

Q09011, doi:10.1029/2005GC000986

ISSN: 1525-2027

Modeling the density at Merapi volcano area, Indonesia, via the inverse gravimetric problem

C. Tiede

Institute of Physical Geodesy, Darmstadt University of Technology, Petersenstrasse 13, D-64287 Darmstadt, Germany (tiede@geod.tu-darmstadt.de)

A. G. Camacho

Instituto de Astronomia y Geodesia (CSIC-UCM), Facultad de Ciencias Matemáticas, Plaza de Ciencias, 3, Ciudad Universitaria, 28040 Madrid, Spain

C. Gerstenecker

Institute of Physical Geodesy, Darmstadt University of Technology, Petersenstrasse 13, D-64287 Darmstadt, Germany

J. Fernández

Instituto de Astronomia y Geodesia (CSIC-UCM), Facultad de Ciencias Matemáticas, Plaza de Ciencias, 3, Ciudad Universitaria, 28040 Madrid, Spain

I. Suyanto

Geophysical Laboratory, Gadja Mada University, Yokyakarta, Indonesia

[1] Merapi is a high-risk andesitic volcano in Central Java, Indonesia. Very little information is known about the detailed regional density structure around Merapi and its neighbor volcano Merbabu. We compute a subsurface three-dimensional (3-D) model of anomalous density for the volcanoes Merapi and Merbabu in Central Java, Indonesia, by inversion of the gravity field. As input for the inversion methodology, gravity observations from 443 points, whose 3-D coordinates are determined by GPS, are used. The inversion algorithm is based on an explorative approach to fit a least squares condition, including a balancing factor between the minimization of the residuals and the anomalous mass. A mean density about 2242 kg/m^3 for the region of Merapi and Merbabu has been computed by least squares adjustment. Results of the inversion show major low-density contrasts up to −242 kg/m^3 and positive structures about +264 kg/m^3, referred to the determined mean density. A density anomaly (relative high) with densities up to +264 kg/m^3 is connecting the volcanoes in a 152° course from NW to SE and might be built of older basaltic lava. Low-density contrasts about −242 kg/m could be found in agreement with magnetotelluric and electromagnetic results. Generally, the identified high- and low-density bodies are in agreement with the results of other geophysical methods such as electromagnetic and magnetotelluric prospecting or geological formations and structures. A porosity about 21% is derived for the largest negative density bodies about −242 kg/m^3. Furthermore, the density model gives some new information about the controversial origin of a hill formation near Merapi and is also used to discuss the possible existence of a shallow magma chamber, which is also a controversial subject. Generally, the density model serves as basic information for the interpretation of geodetic and geophysical observations and confirms existing results from magnetotellurics, electromagnetics, and seismic data interpretation.

Components: 6265 words, 8 figures.

Keywords: density; model; gravity; inversion; Merapi.

Index Terms: 4255 Oceanography: General: Numerical modeling (0545, 0560); 0920 Exploration Geophysics: Gravity methods (1219); 1219 Geodesy and Gravity: Gravity anomalies and Earth structure (0920, 7205, 7240).

Received 31 March 2005; **Revised** 5 July 2005; **Accepted** 20 July 2005; **Published** 10 September 2005.

Tiede, C., A. G. Camacho, C. Gerstenecker, J. Fernández, and I. Suyanto (2005), Modeling the density at Merapi volcano area, Indonesia, via the inverse gravimetric problem, *Geochem. Geophys. Geosyst.*, *6*, Q09011, doi:10.1029/2005GC000986.

1. Introduction

[2] Merapi volcano is located about 300 km north from the Java trench and is one of the most active and hazardous volcanoes worldwide. Around two million people live in its neighborhood [*Setiawan*, 2002] and more than 70,000 in the so-called forbidden zone. Located approximately 30 km away from the volcano is the city of Yokyakarta, with about 500,000 inhabitants. This huge population is permanently threatened by the volcano, which is why Merapi has been classified by the International Association of Volcanology and Chemistry of the Earth's Interior (IAVCEI) as one of 15 high-risk volcanoes in the world within the International Decade for Natural Disaster Reduction of UNESCO.

[3] International research groups from Australia, France, Germany, Italy, Japan, the Netherlands, New Zealand and USA are collaborating with the Volcanological Survey of Indonesia (VSI) and working on Merapi [*Voight et al.*, 2000].

[4] In 1994, Indonesian and German institutions began to cooperate in a project spearheaded and coordinated by the VSI and the GeoForschungsZentrum (GFZ) Potsdam. The Deutsche Forschungsgemeinschaft has been supporting this interdisciplinary research since 1997. The intention of the project MERAPI (Mechanism Evaluation, Risk Assessment, Prediction Improvement) was to increase knowledge on volcanic mechanisms and processes and to improve prediction capabilities. Several subprojects investigate the subsurface structure of Central Java and especially Merapi as well as its neighbor volcano Merbabu [*Zschau et al.*, 1998].

[5] Former gravity inversions resulted in a density profile and a 3-D model for the area of Merapi. A two-dimensional profile for Java is derived from a gravity profile approximately 60 km east of Merapi given by *Sato and Untung* [1978] and gives only vague ideas about the region of Merapi due to its distance. The gravity inversion by *Ritter* [1999] using IGMAS software [*Götze*, 1978, 1984; *Götze and Lahmeyer*, 1988] shows small, local limited structures with densities between 1000 and 4000 kg/m^3. These results are mainly caused by large local limited Bouguer-corrected free air anomalies. With the inversion of our data, which are collected in the region of Merapi, we derive a 3-D density model for the area around Merapi. This model is highly accurate due to the uniform gravity measurements and reduction technique that are used for the inversion.

[6] The 3-D model provides detailed information about the density distribution in the subsurface of the whole area of Merapi and Merbabu, and also about the location, size and shape of main structures such as geological formations or density anomalies found by other observation methods. Density anomalies also may be used to prove the location of a potential shallow magma chamber expected, for example, as a result of seismic experiments or other model attempts such as combined gravity and deformation inversion. Furthermore, the density contrasts lead to a porosity value for the computed density structures that explain electromagnetic or magnetotelluric results. This density model is also used to prove expectations regarding the structure in the area of Merapi. Summarizing, the model is a basis for interpretation and validation of a variety of geophysical and geodetical spatial data such as gravity changes, electromagnetics, magnetotellurics and results of seismic measurements.

2. Geodynamic Framework at Merapi

[7] Merapi (7°32′S, 110°26′E) is an andesitic stratovolcano that is located at the intersection of two fault zones, the NS striking Semarang-fault and the EW located Solo-fault. The volcano is near the subduction zone, where the Indo-Australian plate is moving toward the Eurasian one and is subducted below it. In Java, the convergence is frontal with a velocity of 0.065 m/year [*DeMets et al.*, 1990].

[8] The geology of Central Java [*Gertisser*, 2002], is divided into several structural units: the south coast, including the Karangbolong mountains, the south Seraju chain, and the west Progo mountains, the South mountains, the west foothills of the Solo zone, the north Seraju chain, and the north coast-

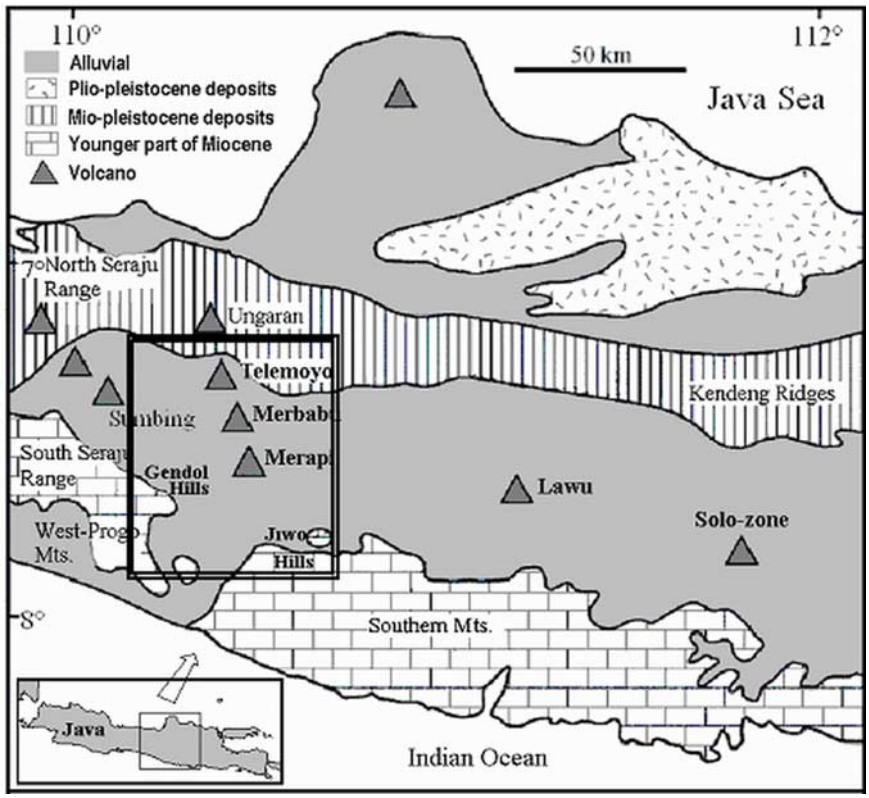

Figure 1. Geology of Central Java after *Van Bemmelen* [1956]. Double square shows the area of observed gravity values.

line; see Figure 1. According to *Van Bemmelen* [1949], the area around Merapi consists of two different materials: The basic material is low-density alluvial, whereas the volcanoes themselves consist of Holocene volcanic material. Merapi, located at the west end of the Solo fault, is the youngest volcano of a volcanic chain beginning in the north with Ungaran and continuing southward over Telemoyo, Merbabu to Merapi. This formation of volcanoes caps the NS striking transverse fault zone [*Van Bemmelen*, 1949]. The density is given as 2000 to 2400 kg/m^3 down to a depth of about 2 km, while at larger depths, a denser material of 2660 kg/m^3 is anticipated [*Sato and Untung*, 1978].

[9] The upper part of Merapi volcano is characterized by a persistent growth of an unstable lava dome at or near the summit [*Newhall et al.*, 2000]. It is built out of highly viscous lava with a silicid acid content between 49.5 and 60.5% [*Camus et al.*, 2000]. The summit structure is essentially formed by loose rocks as well as fractured lava blocks and ash matrix breccia [*Beauducel et al.*, 2000]. In deeper parts, Merapi consists of a sequence of basaltic andesite lavas and pyroclastic deposits of an eroded older volcanic edifice [*Newhall et al.*, 2000].

[10] Using seismic data, the internal structure of Merapi, e.g., the location of a potential magmatic chamber, can be derived due to the different velocity of wave propagation in the material: *Ratdomopurbo and Poupinet* [2000] interpret a zone with anomalous high attenuation of seismic waves 1500–2500 m below the summit as a shallow magma reservoir. However, *Beauducel and Cornet* [1999] did not confirm the existence of such a shallow magma reservoir. The 3-D density model may be used to prove the location of such a magma chamber by comparing the density of the magma chamber to its surroundings.

[11] Magnetotellurics, Long Offset Transient Electromagnetics (LOTEM) as well as NanoTEM investigate the subsurface conductivity. The volcano's hydrothermal system or its magmatic chamber can be detected by performing conductivity contrasts between cold, dry and nonconductive host rock and hot, wet and conductive material, respectively. High conductivity contrasts may be explained by the filling of pore volume with high conductive material, e.g., saline fluids.

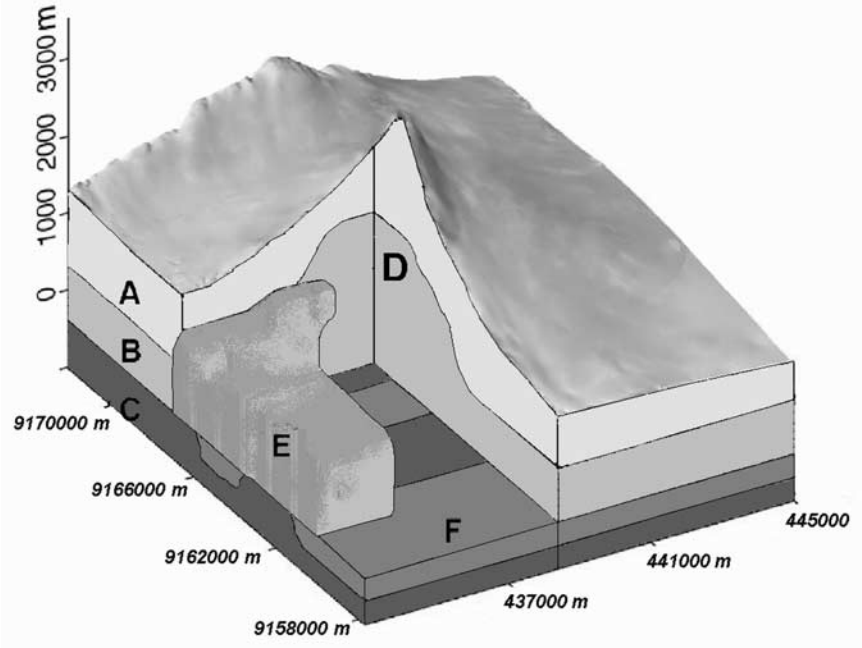

Figure 2. Three-dimensional resistivity model of Merapi determined by the inversion of magnetotelluric measurement after *Müller and Haak* [2004] (with permission from Elsevier). Resistivity values: A, 100 Ωm; B, 10 Ωm; C, 1 Ωm; D, 10 Ωm; E, <1 Ωm. F represents two 2-D regional structures extending beyond the volcano with a resistivity of 0.1 Ωm. UTM coordinates in meters for horizontal axis.

The porosity values derived from conductivity can be testified by the density model. Therefore the density contrasts are explained by an exchange of a certain percentage of material with saline fluid density. So a porosity value may be obtained. The 3-D magnetotellurics forward modeling results including the topography are given by *Müller and Haak* [2004] and show five different resistivity layers and bodies respectively (Figure 2). Of these five, the most interesting for this study are given by a high electric radial symmetric conductor (D) below the summit of Merapi. It has a resistivity of 10 Ωm and approximately follows the topography with its upper boundary between 1000 to 1600 m below the surface. The second body of interest is given by (E) which describes a high conductive body with a resistivity of 1 Ωm as an upper estimation that is located about four km SW of the summit, 300 m below the surface.

[12] LOTEM observations focus on detecting the conductivity structures below the summit region. Results show a strong monotonous resistivity that decreases with increasing depth [*Commer et al.*, 2005]. This result coincides with conclusions drawn from DC resistivity imaging along the volcano's flanks [*Friedel et al.*, 2000]. Furthermore, a high conductive layer dislocation of about 7700 m south of the summit has been observed by LOTEM measurements [*Müller et al.*, 2002; *Kalscheuer*, 2004] and NanoTEM [*Koch*, 2003]. Also a high conductive body west of Merapi at a depth of about several hundred meters was identified.

[13] *Setiawan* [2002] concludes "that in the subsurface (of Merapi) a high pore volume is existing, maybe 10%–20%," derived from small density values between 2000 and 2400 kg/m^3 assumed by *Wegler et al.* [2000]. After *Angenheister* [1982], porosity values up to 15% are realistic values for volcanic regions. Porosity estimations of the low resistivity below the summit result in values of about 5(10)% by anticipating a bulk resistivity of 0.7 Ωm and a NaCl concentration of 25(10) equivalent weight%, *Commer et al.* [2005]. 10(20)% are also necessary to explain the fluid resistivity values of 0.2(1) Ωm, measured by LOTEM [*Müller et al.*, 2002].

[14] Except for the magnetotellurics modeling with a large exploration depth [*Müller and Haak*, 2004], the described measurements allow only a local density interpretation [see, e.g., *Beauducel and Cornet*, 1999; *Beauducel et al.*, 2000; *Ratdomopurbo and Poupinet*, 2000; *Wegler and Lühr*, 2001]. So there is still very little knowledge about the density subsurface structure around

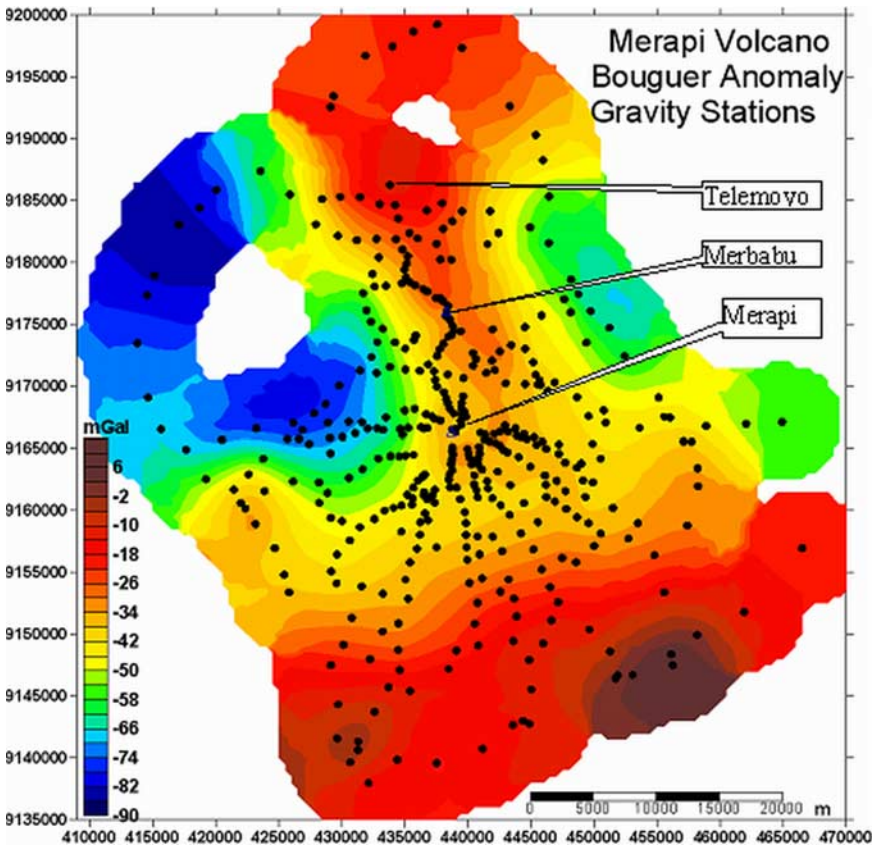

Figure 3. Bouguer-corrected free air gravity anomaly and location of the 443 GPS and gravity observation points used. Color scale in mGal. Axis with UTM coordinates (zone 49S) in meters. The positions of three volcanoes in the area are indicated.

Merapi and Merbabu, and no 3-D and regional density model for Merapi region is derived yet.

3. Data Sets and Processing

[15] Two sources of combined gravity and GPS observations for the Merapi area exist. The first data set of 529 points was published by *Jousset* [1996]. This data set consists of all accessible data in that region. Gravity point positions are mainly taken from topographic maps and barometric altitude measurements. The second data set, consisting of 443 points, was measured in winter 1996/1997 by Darmstadt University of Technology, Institute of Physical Geodesy in cooperation with the Geophysical Laboratory of Gadjah Mada University, with a Lacoste&Romberg gravity meter. 3-D coordinates of the gravity points have been measured by two-frequency GPS receivers.

[16] The first data source has not been considered in the following inversion approach due to its lack of any error estimation, thus preventing a weighted fusion of the two data sets. Furthermore, the determination of coordinates, especially of the altitudes, results in certain high levels of uncertainty. Results of inversion are small sized bodies with too large density anomalies.

[17] GPS and gravity data processing of the second data source is described in the Appendix. Figure 3 gives an overview about the computed Bouguer-corrected free air anomaly $\delta \mathbf{g}_{BCFA}$ we use in our study. $\delta \mathbf{g}_{BCFA}$ is negative in the west and east and positive in the south as well as around the center of the volcanoes Merbabu and Merapi in the middle, increasing from south to north. According to *Sato and Untung* [1978], residual gravity anomalies that reflect undulations of deep density discontinuity show a clear negative anomaly in the east of Merapi, and a clear positive anomaly in the south that confirms our computed gravity anomalies.

4. Inversion Methodology

[18] Figure 3 suggests several features about the horizontal changes in mass distribution of the region. Nevertheless, more valuable information

can be obtained from a gravity inversion of the anomaly, seeking the location and geometric size of the subsurface mass anomalies that might produce the gravity anomaly observed on the surface. The nonuniqueness problem of the gravity inversion is well known [*Al-Chalabi*, 1971]. Nevertheless, valuable particular solutions can be obtained by including additional constraints about subsurface structure (with a geological base and some statistical formulism) and the data statistical properties. The inversion methods that determine the geometrical properties of anomalous bodies with prescribed density contrast [*Barbosa et al.*, 1997; *Pedersen*, 1979] correspond to a nonlinear context. They can offer interesting morphological results whose validity is conditioned by the validity of the particular hypothesis (density contrast, geometrical elements or describe the model, etc.) used. For the fully nonlinear treatment, the methods of exploration of the space model often provide the best option [*Tarantola*, 1988]. This exploration process can be conducted randomly [*Silva and Hohmann*, 1983] or systematically. *Camacho et al.* [2000, 2002] developed a 3-D gravity inversion method by means of a growth process for the bodies, which are responsible for the gravity anomalies. They are defined by means of aggregation of small parallelepiped cells filled with a prescribed anomalous mass. An exploratory approach permits the construction of the anomalous bodies as step-by-step aggregation of prismatic cells. The gravitational attraction, A_{ij}, at the *i-th* station $P_i(x_i; y_i; z_i)$, due to the *j-th* prism, for unit density, is given by *Pick et al.* [1973]:

$$A_{ij} = -G\left[\left[\left[x\ln\left(y+\left(x^2+y^2+z^2\right)^{1/2}\right)+y\ln\left(x+\left(x^2+y^2+z^2\right)^{1/2}\right)+z\,\mathrm{arctg}\left(z\left(x^2+y^2+z^2\right)^{1/2}x^{-1}y^{-1}\right)\right]_{u_1^j-x_i}^{u_2^j-x_i}\right]_{v_1^j-y_i}^{v_2^j-y_i}\Bigg]_{w_1^j-z_i}^{w_2^j-z_i} \quad (1)$$

where G is the gravitational constant, the edges of the *j-th* prism are parallel to the reference axes of the coordinate system, and the limiting coordinates for its volume are: u_1^j, u_2^j for the x coordinates, v_1^j, v_2^j for the y coordinates and w_1^j, w_2^j for z. The process starts by selecting a partition of the subsurface volume in prismatic cells. Furthermore, a fixed (positive and/or negative) density contrast is selected for use in constructing the adjusted anomalous structures. Next, the anomalous bodies are reconstructed by growth or adding from the first filled cells until a volume of aggregated cells filled with the (positive and/or negative) prescribed anomalous density is completed. For each step of this growth process, a suitable cell is selected (to be filled) by means of an exploratory process throughout the unfilled cells. During the growth process, the growing bodies look to minimize the gravity residual vector $\boldsymbol{\nu}$, calculated as the difference between the Bouguer-corrected free Air anomalies δg_{BCFA} that were determined from the observed gravity values and the scaled model gravity values $f\Delta g_c$, where $f \geq 1$ is a suitable scale factor. The growth process stops when $f = 1$. If only a minimization criterion for the residuals $\mathbf{v}$ is used, the acceptance of positive and negative values for the prescribed density contrasts (and the inclusion of regional trend unknowns) gives an inherent nonuniqueness problem. To solve this, an additional condition of minimization of the model variation is adopted. Thus the solution is obtained by a mixed condition formed by the gravity l_2 fitness and the whole anomalous mass quantity, using a parameter λ for the suitable balance:

$$\mathbf{v}^T\mathbf{Q}_D^{-1}\mathbf{v} + \lambda\mathbf{m}^T\mathbf{Q}_M^{-1}\mathbf{m} = \min \quad (2)$$

$\mathbf{v} = (v_1;\ldots;\ v_N)^T$ are the residuals (Bouguer-corrected free air anomalies minus modeled values) computed out of the gravity observations for the N stations, $\mathbf{m} = (\Delta\rho_1\ \ldots\ \Delta\rho_m)^T$ are the anomalous densities (positive, negative and/or zero) for the m cells of the subsoil partition, and λ is a positive factor, empirically fixed, for balance between model fitness and anomalous model magnitude (and complexity). $\mathbf{Q}_D$ is the covariance matrix (usually uncorrelated) corresponding to the estimated (Gaussian) inaccuracies of the gravity data, and $\mathbf{Q}_M$ is the covariance matrix corresponding to the supposed determinability of the model parameters $\mathbf{m}$. The first addend of the minimization functional given in equation (2) corresponds to the fit residuals weighted with the data quality matrix (gravity data variances from the observation analysis). The second addend is a weighted addition of the model densities, subsequently connected with the whole anomalous mass or magnitude of the model. The final model is a 3-D structure described by aggregation of the cells with anomalous density contrasts, and can be viewed as vertical sections and horizontal profiles. This structure must be accepted as a particular model corresponding to the observed gravity values, the supposed data noise and the choice of balance λ between model fitness vs. model smoothness.

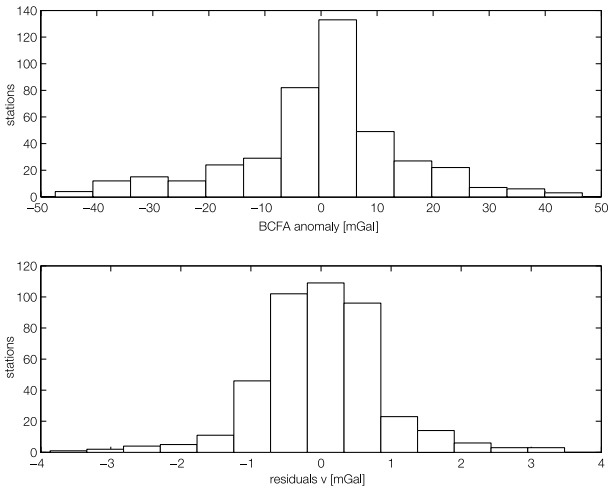

Figure 4. Histograms showing the observed Bouguer-corrected free air (BCFA) gravity anomalies as well as the residuals **v** between observed and modeled values $\delta\mathbf{g}_{BCFA}$ of 443 observed stations.

Moreover, general regional stratification for the subsurface volume is not drawn. In fact, gravity is not sensitive to horizontal stratification. Thus the adjusted model corresponds to anomalous density structures with respect to a mean subsurface normal structure, not necessarily homogeneous, with any horizontal stratification but without lateral discontinuities.

5. Results

[19] The gravity inversion model is formed by about 20,000 cells. The filled cells (for prior adopted density contrasts between extremal values -300 kg/m^3 and $+300$ kg/m^3) describe a 3-D model of geometrical distribution for anomalous structures, with resulting mean anomalous densities of -242 kg/m^3 and 262 kg/m^3.

[20] The fit of the model is given by the histogram showing the residuals **v**, Figure 4, as well as by the weighted root mean square (rms). The posterior RMS is $((\mathbf{v}^T\mathbf{Q}_D^{-1}\mathbf{v})/N)^{0.5} = 0.046$ mGal, compared to a prior RMS about $((\delta\mathbf{g}_{BCFA}^T\mathbf{Q}_D^{-1}\,\delta\mathbf{g}_{BCFA})/N)^{0.5} = 0.504$ mGal, with $N = 443$ number of observed gravity values.

[21] The following list gives the most interesting areas with the resulting large anomalous density contrasts; see Figures 5 (3-D view of low-density bodies), 6 (3-D view of high-density bodies), 7 (horizontal sections), and 8 (horizontal and vertical profile for central structure). Coordinates are based on UTM and the depth on EGM96 geoid.

[22] (a) In Figures 5 and 7: Body with a low density. East (417000–434500 m), north (9162000–9176500 m), depth between -9000 and 0 m. The 2-D location is in agreement with the high conductive body (E) found by magnetotellurics.

[23] (b) In Figure 5: Low-density body below Merapi at a depth of approximately +1100 to +2100 m. East (439000–441500 m) and north (9165500–9168500 m). This body coincides in east as well as north coordinates with the results according to *Müller and Haak* [2004], body (D),

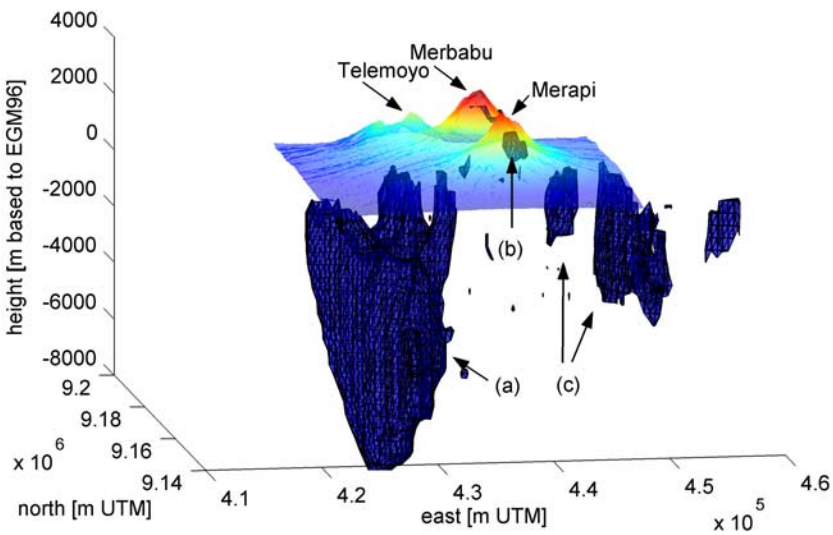

Figure 5. Three-dimensional view from SE direction to isosurfaces with a negative density contrast about -200 kg/m^3. Discussed negative density contrasts are named (a), (b), and (c). The three volcanoes are indicated.

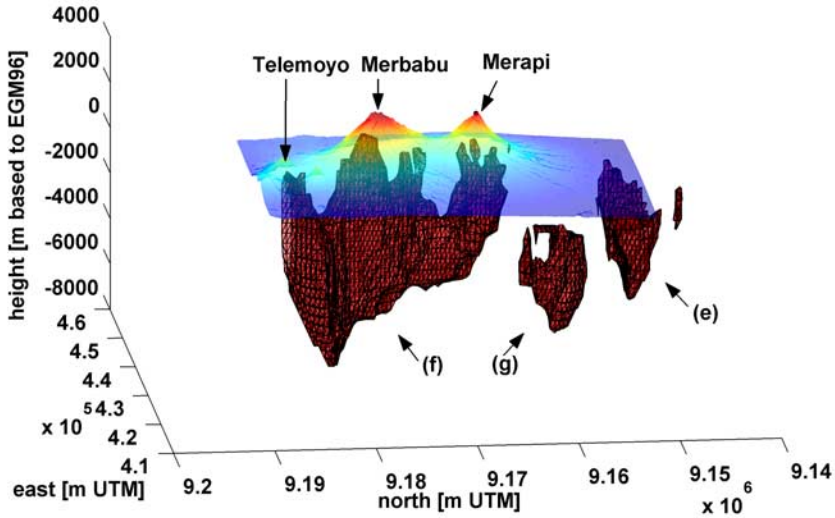

Figure 6. Three-dimensional view from N direction to isosurfaces with positive density contrast about +200 kg/m^3. Discussed positive density contrasts are named (e), (f), and (g). The three volcanoes are indicated.

whereby the height is determined more shallow for this body by the gravity inversion.

[24] (c) In Figures 5 and 7: Low-density bodies east of Merapi arranged in an arc with a concave shape to Merapi. East (444500–454000 m), north (9157000–9185500 m), depth between −6000 and 0 m. It is touching an area of negative Bouguer-corrected free air anomalies, which are equivalent to low densities, described by *Sato and Untung* [1978].

[25] (d) In Figure 7: Small low-density body with WE extension southward of Merapi for a distance of about 8 km, striking from west to east. East (438000–445000 m), north (9157000–9160500 m), depth between −4000 and −1500 m. This body coincides in its location with the high conductive body found by LOTEM observations [*Müller et al.*, 2002; *Kalscheuer*, 2004] and Nano-TEM [*Koch*, 2003]. The large depth extension of the body would confirm the expectation of a vertical fault structure [*Kalscheuer*, 2004; *Commer et al.*, 2005] to explain the LOTEM measurements whereby former LOTEM models do not take this fault structure into account and result in conductivity extending vertically for only a few hundred meters.

[26] (e) In Figures 6 and Figure 7: Positive density contrast chain. East (428000–460000 m), north (9140000–9153000 m) and a depth between −6000 and 0 m. The location of the high-density chain can be correlated with a longitudinal fault system that is originating between the Solo zone and the Southern Mountains, as well as with a part of the central depression zone of Java [*Van Bemmelen*, 1949]. Furthermore, this region also covers the Jiwo Hills, a fossiliferous seabed, discordantly overlying strongly folded pre-Tertiary schists.

[27] (f) In Figures 6 and 7: Arc along volcanoes with a high density: East (429000–444000 m), north (9167000–9188000 m), depth between −7000 and +2000 m showing the connection of the volcanoes and the continuation of the NS striking transverse fault zone that is mentioned by *Van Bemmelen* [1949]. This connection of the volcanoes Merapi, Merbabu and Telemoyo in the north underlines the history of the volcanic origin and might show the older basaltic lavas underlying the newer deposits. The morphology given by the adjusted model suggest an intrusive complex starting from the large positive body on the NW border, and running in direction 152° N to the SE across the volcanoes and with a mean depth of about −2000 m. Several small, shallower bodies are to be seen across the elongated body, such as the one connecting the main course with the location of Merapi in the SE corner.

[28] (g) In Figures 6 and 7: Positive density contrast, east (418500–425000 m), north between 9156000–9163500 m at a depth between −4000 m and 0 m in the region where the Gendol hills are located. These hills are described as the folded foot of the old Merapi [*Van Bemmelen*, 1949]. *Newhall et al.* [2000] believe that these hills are ‘‘erosional rem-

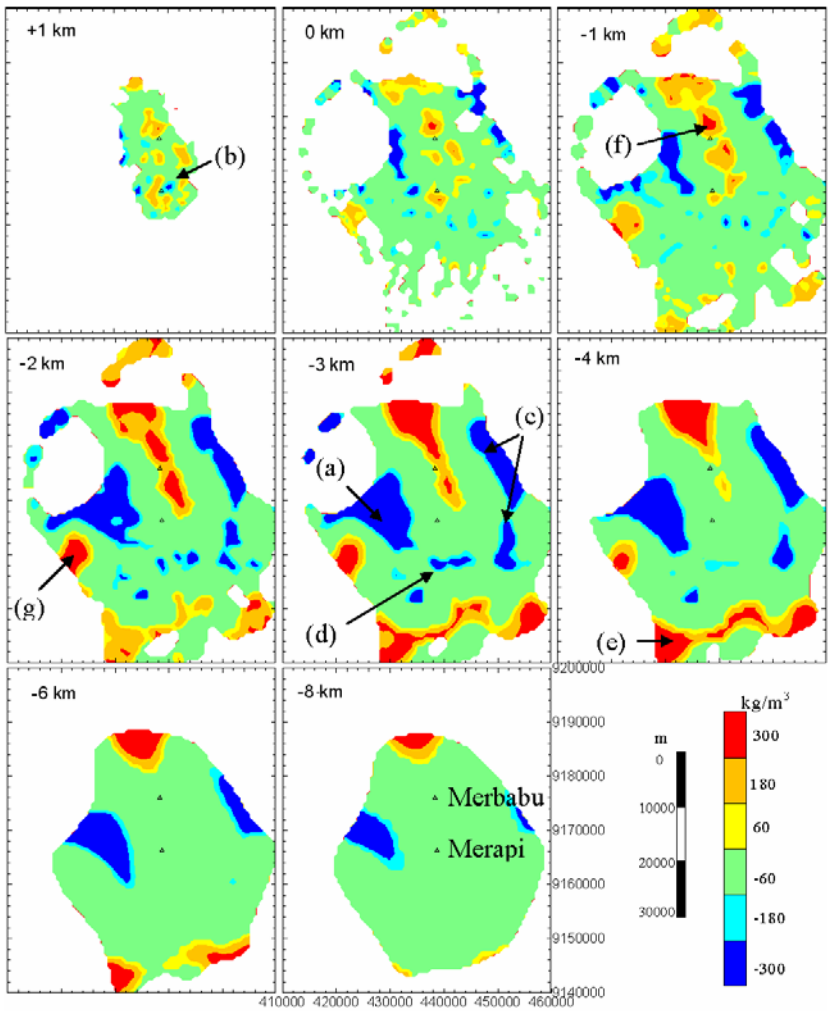

Figure 7. Horizontal sections of the 3-D model of anomalous density contrast from +1000 m to −8000 m ASL. Axes with UTM coordinates are similar for each of the eight subplots. Letters (a)–(g) correspond to several characteristic bodies of anomalous high- or low-density contrasts. Small triangles give the positions of Merapi and Merbabu volcanoes.

nants of pre-Merapi volcanoes, and are not from a landslide-like 'slip faulting' or debris avalanche of Merapi.'' *Camus et al.* [2000] interpret the Gendol hills as ''the visible parts of the debris avalanche deposit, protruding from thick, younger pyroclastic deposits.'' Assuming that the higher densities are caused by older basaltic material of the pre-avalanche period and that (g) is not connected to the high-density anomalies below the volcanoes (f), as well as that no other high-density bodies exist in this area, the density model would thus further support the version of the Gendol hills not being related to volcanic activity.

[29] Generally we can estimate porosity values from density contrasts: To compute a porosity value for the bodies (a), (b), (c), and (d) of the density model, we assume that the pores are filled completely with saline fluids of a density of 1090 kg/m^3. The largest occurring density changes in these bodies of −242 k/m^3 would postulate a porosity of 21%. Such high porosities for the whole volcanic region are also assumed for gravity modeling [*Setiawan*, 2002]. In addition *Commer et al.* [2005] suggest a porosity of 5(10)% for a bulk resistivity of 0.7 Ωm found for the central volcanic complex and a NaCl equivalent weight percent of 25(10). The low-density body (b) of our model would suggest the derived lower concentration of NaCl for this area.

[30] Our data could not confirm the anticipated aseismic zone between 1500 and 2500 m below the summit. Body (b) lies approximately in this region, 800–1800 m below the summit, 50 m east and 1000 m south of it. But to draw any conclusion

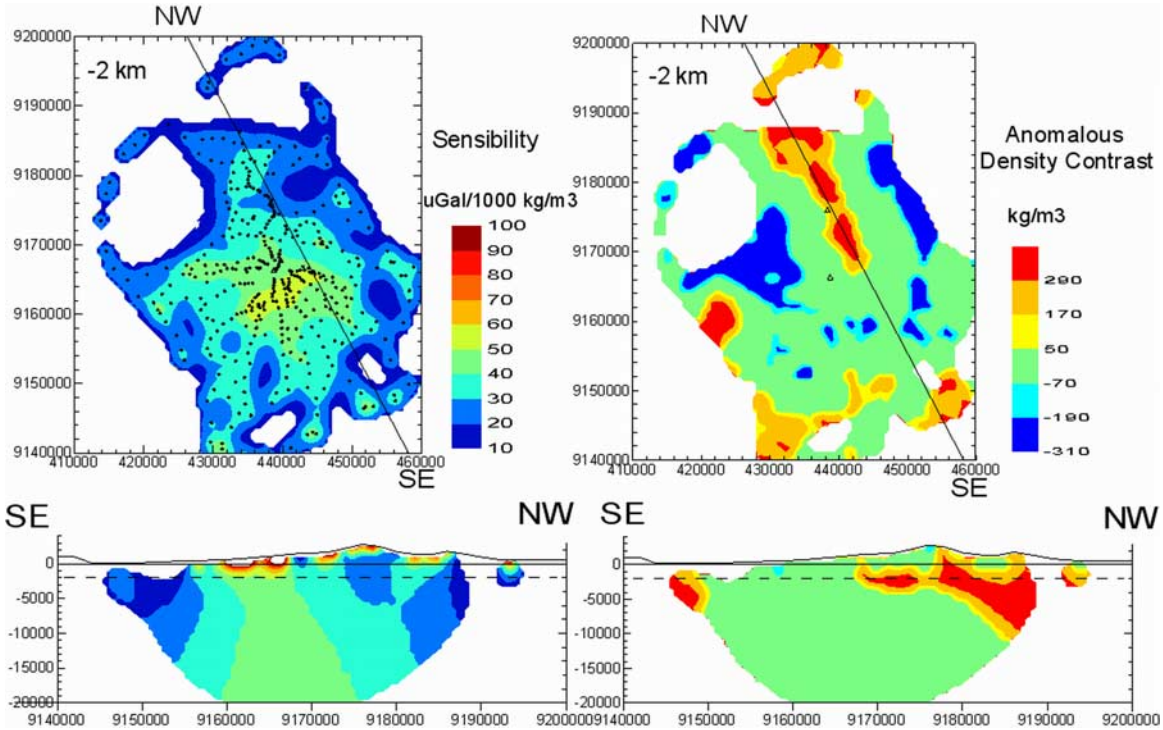

Figure 8. Horizontal and vertical cross sections of the 3-D anomalous density model (right) and sensitivity distribution of the model (left). UTM coordinates. The vertical SE-NW profiles follow the 152°N course of the intrusive body (f). The sensitivity pattern corresponds to the station distribution and the relative size and position of the 20,000 cells.

about this relation would be very vague, so our data do not confirm the anticipated shallow magma chamber.

[31] The inverse model comes from the fit of 443 data points by means of a structure defined by about 20,000 parallelepiped cells (each with a side of about 800 m), mostly filled with the prior selected density values. We can gain an idea of the relative precision of the individual cells by plotting the sensitivity of the gravity data, as given by the root mean square attraction for a fixed density contrast, for different cells. Figure 8 shows two profiles of this sensitivity distribution. A value of 40 μGal for density contrast 1000 kg/m^3 can be given as a mean benchmark.

6. Summary and Conclusions

[32] A detailed density model for the area of Merapi volcano, Central Java, Indonesia was computed by the inversion of gravity anomalies. Gravity and GPS observations at 443 points around Merapi and Merbabu served as input data.

[33] A mean density of 2242 kg/m^3 for this region was obtained. Results of the inversion algorithm show density contrasts between 2000 and 2504 kg/m^3. A high conductive body derived from magnetotellurics in the west of Merapi is identified as a low-density body with our model. In addition, our model proves the high conductive body that was found by LOTEM and NanoTEM in the south of Merapi. Furthermore a connective body below the volcanoes that might consist of older basaltic lavas was found underlying the newer deposits.

[34] A porosity value is derived from the largest occurring low-density anomaly of −242 kg/m^3. A porosity value of 21% is obtained by filling the whole pore volume of 21% with saline fluids of a density of 1090 kg/m^3, anticipating the mean density of 2242 kg/m^3 for the remaining 79%. This porosity is likely to occur within the low-density bodies (a), (b), (c), and (d).

[35] Our density model could not confirm the magma chamber assumed by seismic experiments 1500–2500 m below the summit.

[36] The density model gives certain information about the origin of the Gendol hills that has been controversially discussed in former studies.

According to our results, these hills might not be related to a volcanic event in the Middle Merapi period.

[37] Summarizing, this model could be used to prove existing results and give some information about controversially discussed structures as well as porosity estimations for the region. Furthermore, this density model is basic information for further interpretation of geodetic and geophysical data at Merapi and gives a homogenous density modeling result that is physically reliable and matches observations from other techniques carried out at Merapi.

Appendix A: Description of the GPS and Gravity Data Processing Methodology

[38] The corresponding GPS data were processed using precise ephemerides. Baselines are up to 30000 m long. The standard deviation of horizontal position is $\leq \pm 0.03$ m, and of height $\leq \pm 0.10$ m, respectively. The accuracy of the adjusted gravity data is estimated as ±0.010 mGal (1 mGal = $1 \cdot 10^{-5}$m/s^2) for repeatedly observed points and ±0.040 mGal for all the others.

[39] The ellipsoidal heights were converted to orthometric heights by the computation of the geoid undulation of the EGM96 gravity model [*Lemoine et al.*, 1998]. The complete reduction of the gravity data consists of the following steps:

[40] 1. Computation of the normal gravity (γ_0) referenced to GRS80 [*Moritz*, 2000] as

$$\gamma_0 = 978032.67715\left(1 + 0.0052790414\ \sin^2\phi + 0.0000232718\sin^4\phi + 0.0000001262\sin^6\phi + 0.0000000007\sin^8\phi\right) \quad \text{(A1)}$$

with ϕ being the latitude of observation point in degrees.

[41] 2. Computation of the gravity anomaly (δg_{EGM96}), based on the spherical harmonic expansion related to the EGM96 with a resolution to degree and order of 360.

[42] 3. Computation of the free air correction (δg_F) in mGal:

$$\delta g_F = 0.30877\left(1 - 0.00142\sin^2\phi\right)h \quad \text{(A2)}$$

with h being the orthometric height of observation point in meters.

[43] 4. Computation of the topographic effects (δg_{top}) on gravimetric quantities for a unique density of 1000 kg/m^3 [*Forsberg*, 1984].

[44] The topographic effects were determined by computing the gravitational attraction of the topography represented by orthogonal prisms. Therefore a hybrid digital elevation model was developed which consists of the Sandwell bathymetric model (grid spacing = $2' \times 2'$) [*Smith and Sandwell*, 1997] and the SRTM data (grid spacing = $30'' \times 30''$) in the far range, and a local digital elevation model for the area of Merapi and Merbabu, computed from photogrammetric and INSAR-data (grid spacing = $0.5'' \times 0.5''$) [*Läufer*, 2003] in the near range.

[45] The Bouguer-corrected free air anomaly (δg_{BCFA}) is then

$$\delta g_{BCFA} = g_{obs} + \delta g_F - \rho_{top}\delta g_{top} - \gamma_0 - \delta g_{EGM96} \quad \text{(A3)}$$

with g_{obs} being observed gravity in mGal. The density ρ_{top} is determined together with a regional trend by least squares adjustment, as proposed by *Torge* [1989]:

$$v_i = a\lambda_i + b\phi_i + \gamma_{0i} + \rho_{top}\delta g_{top} - \delta g_F - g_{obs} \quad \text{(A4)}$$

a and b are coefficients for a linear regional trend, index i starts for values corresponding to the i-th station with geodetic coordinates (ϕ_i, λ_i), v_i are residuals and $\rho_{top}\delta g_{top}$ represents topographic reduction with respect to the mean unknown topographic density ρ_{top}.

[46] The least squares adjustment according to equation (A4) results in a mean density ρ_{top} of 2242 ± 29 kg/m^3 and a regional trend $y = 0.00661\ (\pm 0.00078)\lambda - 0.00036\ (\pm 0.00004)\ \phi$ [mGal].

Acknowledgments

[47] Field measurements and research stay of IS in Germany have been supported by the International Office at DLR, under INO-009-96. The research by AGC and JF has been funded under MCyT project REN2002-03450. We want to thank M. Commer as well as an anonymous reviewer for their valuable reviews of this paper.

References

Al-Chalabi, M. (1971), Some studies relating to non-uniqueness in gravity and magnetic inverse problem, *Geophysics*, *36*(5), 835–855.

Angenheister, G. (1982), Physical properties of rocks, in *Landolt-Börnstein Numerical Data and Functional Relationships in Science and Technology*, *Geophys. Space Res.*, vol. 2,

edited by K.-H. Hellwege, pp. 184–303, Springer, New York.

Barbosa, V. C. F., J. B. C. Silva, and W. E. Medeiros (1997), Gravity inversion of basements relief using approximate equality constraints on depths, *Geophysics*, *62*(6), 1745–1757.

Beauducel, F., and F. H. Cornet (1999), Collection and three-dimensional modeling of GPS and tilt data at Merapi volcano, Java, *J. Geophys. Res.*, *104*, 725–736.

Beauducel, F., F. H. Cornet, E. Suhanto, T. Duquesnoy, and M. Kasser (2000), Constraints on magma flux from displacements data at Merapi volcano, Java, Indonesia, *J. Geophys. Res.*, *105*, 8193–8204.

Camacho, A. G., F. G. Montesinos, and R. Vieira (2000), Gravity inversion by means of growing bodies, *Geophysics*, *65*, 95–101.

Camacho, A. G., F. G. Montesinos, and R. Vieira (2002), A 3-D gravity inversion tool based on exploration of model possibilities, *Comput. Geosci.*, *28*, 191–204.

Camus, G., A. Gourgaud, P.-C. Mossand-Berthommier, and P.-M. Vincent (2000), Merapi (Central Java, Indonesia): An outline of the structural and magmatological evolution, with a special emphasis to the major pyroclastic events, *J. Volcanol. Geotherm. Res.*, *100*, 139–163.

Commer, M., S. L. Helwig, A. Hördt, and B. Tezkan (2005), Interpretation of long-offset transient electromagnetic data from Mount Merapi, Indonesia, using a three-dimensional optimization approach, *J. Geophys. Res.*, *110*, B03207, doi:10.1029/2004JB003206.

DeMets, C., R. G. Gordon, D. F. Argus, and S. Stein (1990), Current plate motion, *Geophys. J. Int.*, *101*, 425–478.

Forsberg, R. (1984), A study of terrain reductions, density anomalies and geophysical inversion methods in gravity field modeling, *Rep. 355*, Dep. of Geod. Sci., Ohio State Univ., Columbus.

Friedel, S., I. Brunner, F. Jacobs. and C. Rücker (2000), New results from DC resistivity imaging along the flanks of Merapi Volcano, in *Decade-Volcanoes Under Investigation*, edited by J. Zschau and M. Westerhaus, vol. IV/2000, pp. 23–29, Dtsch. Geophys. Ges., Potsdam, Germany.

Gertisser, R. (2002), Gunung Merapi (Java, Indonesien): Eruptionsgeschichte und magmatische Evolution eines Hoch-Risikovulkans, Ph.D. thesis, Geowissenschaftliche Fakultät, Albert-Ludwigs-Universität Freiburg, Freiburg, Germany.

Götze, H.-J. (1978), Ein numerisches Verfahren zur Berechnung der gravimetrischen Feldgrö(en drei-dimensionaler Modellkörper, *Arch. Meteorol. Geophys. Bioklimatol., Ser. A*, *25*, 195–215.

Götze, H.-J. (1984), Über den Einsatz interaktiver Computergraphik im Rahmen 3-dimensionaler Interpretationstechniken in Gravimetrie und Magnetik, Habilitations-Schrift, Tech. Univ. Clausthal, Clausthal, Germany.

Götze, H.-J., and B. Lahmeyer (1988), Application of three-dimensional interactive modelling in gravity and magnetics, *Geophysics*, *53*(8), 1096–1108.

Jousset, P. (1996), Gravimétrie et microgravimétrie en volcanologie: Méthodologie et application au volcan Merapi, Java, Indonésie, Ph.D. thesis, 325 pp., Univ. Denis Diderot-Paris VII.

Kalscheuer, T. (2004), Die Auswertung der LOTEM-Daten vom Südhang des Merapi, diploma thesis, Univ. of Cologne, Cologne, Germany.

Koch, O. (2003), Transient-elektromagnetische Messungen zur Erkundung einer Leitfähigkeitsanomalie am Vulkan Merapi in Indonesien, diploma thesis, Univ. of Cologne, Cologne, Germany.

Läufer, G. (2003), Erzeugung hybrider digitaler Höhenmodelle aktiver Vulkane am Beispiel des Merapi, Indonesien, Ph.D. thesis, Darmstadt Univ. of Technol., Darmstadt, Germany.

Lemoine, F. G., et al. (1998), The development of the Joint NASA GSFC and the National Imagery and Mapping Agency (NIMA) Geopotential Model EGM96, NASA Goddard Space Flight Cent., Greenbelt, Md.

Moritz, H. (2000), Geodetic Reference System 1980, *J. Geod.*, *74*, 128–133.

Müller, A., and V. Haak (2004), 3-D modelling of a conductivity structure: Integrating magnetotellurics, induction vectors and the effect of steep topography—A case study from Merapi volcano (Central Java), *J. Volcanol. Geotherm. Res.*, *138*(3–4), 205–222.

Müller, M., A. Hördt, and F. M. Neubauer (2002), Internal structure of Mount Merapi, Indonesia, derived from long-offset transient electromagnetic data, *J. Geophys. Res.*, *107*(B9), 2187, doi:10.1029/2001JB000148.

Newhall, C. G., S. Bronto, B. Alloway, N. G. Banks, I. Bahar, and M. A. D. Marmol (2000), 10000 years of explosive eruptions of Merapi Volcano, Central Java: Archaeological and modern implications, *J. Volcanol. Geotherm. Res.*, *100*, 9–50.

Pedersen, L. B. (1979), Constrained inversion of potential field data, *Geophys. Prospect.*, *27*, 726–748.

Pick, M., J. Picha, and V. Vyskôcil (1973), *Theory of the Earth's Gravity Field*, Elsevier, New York.

Ratdomopurbo, A., and G. Poupinet (2000), An overview of the seismicity of Merapi volcano (Java, Indonesia) 1983–1994, *J. Volcanol. Geotherm. Res.*, *100*, 193–214.

Ritter, A. (1999), Modellierung der Untergrundstruktur des Merapi-Merbabu Vulkankomplexes, diploma thesis, Darmstadt Univ. of Technol., Darmstadt, Germany.

Sato, Y., and M. Untung (1978), Gravity and geological studies in Jawa, Indonesia, Geol. Surv. of Indonesia/Geol. Surv. of Jpn.

Setiawan, A. (2002), Modelling of gravity changes on Merapi volcano observed between 1997–2000, Ph.D. thesis, Darmstadt Univ. of Technol., Darmstadt, Germany.

Silva, J. B. C., and G. W. Hohmann (1983), Nonlinear magnetic inversion using a random search method, *Geophysics*, *46*(12), 1645–1658.

Smith, W. H. F., and D. T. Sandwell (1997), Global seafloor topography from satellite altimetry and ship depth soundings, *Science*, *277*, 1957–1962.

Tarantola, A. (1988), *The Inverse Problem Theory: Methods for Data Fitting and Model Parameter Estimation*, Elsevier, New York.

Torge, W. (1989), *Gravimetry*, de Gruyter, New York.

Van Bemmelen, R. W. (1949), *The Geology of Indonesia: General Geology*, Govt. Print. Off., The Haque, Amsterdam.

Van Bemmelen, R. W. (1956), The influence of geologic events on human history (an example from Central Java), *Verh. Kon. Ned. Geol. Mijnb. Genoot. Geol.*, *16*, 20–36.

Voight, B., R. Sukhyar, and A.-D. Wirakusumah (2000), Introduction to the special issue on Merapi Volcano, *J. Volcanol. Geotherm. Res.*, *100*, 1–8.

Wegler, U., and B.-G. Lühr (2001), Scattering behaviour at Merapi volcano (Java) revealed from an active seismic experiment, *Geophys. J. Int.*, *145*, 579–592.

Wegler, U., B.-G. Lühr, J. Zschau, N. Maercklin, C. Riedel, and W. Rabbel (2000), Multiple seismic scattering effect at Mount Merapi—Active seismic measurements help to explain complex earthquakes signal of strato volcano, in *Decade-Volcanoes Under Investigation*, edited by J. Zschau

and M. Westerhaus, vol. IV/2000, pp. 43–48, Dtsch. Geophys. Ges., Potsdam, Germany.

Zschau, J., R. Sukhyar, M. Purbawinata, B. Lühr, and M. Westerhaus (1998), Project Merapi—Interdisciplinary research at a high-risk volcano, *Decade Volcanoes Under Investigation*, edited by J. Zschau and M. Westerhaus, Vol. III/1998, pp. 3–8, Dtsch. Geophys. Ges., Potsdam, Germany.